LANGMUIR Cite This: *Langmuir* 2018, 34, 13296−13304 Article pubs.acs.org/Langmuir

Electron Paramagnetic Resonance and Small-Angle X-ray Scattering Characterization of Solid Lipid Nanoparticles and Nanostructured Lipid Carriers for Dibucaine Encapsulation

Raquel M. Barbosa,*[,†,‡] Bruna R. Casadei,[§] Evandro L. Duarte,[⊥] Patrícia Severino,[∥] Leandro R. S. Barbosa,[⊥] Nelson Duran,[#] and Eneida de Paula[†]

[†]Biochemistry and Tissue Biology Department, Institute of Biology, University of Campinas (UNICAMP), 13083-862 Campinas, São Paulo, Brazil

[#]Institute of Chemistry, University of Campinas (UNICAMP), 13083-861 Campinas, São Paulo, Brazil

[‡]Pharmacy Department, UNINASSAU College, 59080-400 Natal, Rio Grande do Norte, Brazil

[§]Biophysics Department, Federal University of São Paulo (UNIFESP), 04021-001 São Paulo, São Paulo, Brazil

[∥]Laboratory of Nanotechnology and Nanomedicine (LNMED), Tiradentes University (UNIT) and Institute of Technology and Research (ITP), Av. Murilo Dantas, 300, 49010-390 Aracaju, Sergipe, Brazil

[⊥]Physics Institute, University of São Paulo (USP), 05508-090 São Paulo, São Paulo, Brazil

ABSTRACT: Dibucaine (DBC) is one of the most potent long-acting local anesthetics, but it also has significant toxic side effects and low water solubility. Solid lipid nanoparticles (SLNs) and nanostructured lipid carriers (NLCs) have been proposed as drug-delivery systems to increase the bioavailability of local anesthetics. The purpose of the present study was to characterize SLNs and NLCs composed of cetyl palmitate or myristyl myristate, a mixture of capric and caprylic acids (for NLCs only) plus Pluronic F68 prepared for the encapsulation of DBC. We intended to provide a careful structural characterization of the nanoparticles to identify the relevant architectural parameters that lead to the desirable biological response. Initially, SLNs and NLCs were assessed in terms of their size distribution, morphology, surface charge, and drug loading. Spectroscopic techniques (infrared spectroscopy and electron paramagnetic resonance, EPR) plus small-angle X-ray scattering (SAXS) provided information on the interactions between nanoparticle components and their structural organization. The sizes of nanoparticles were in the 180 nm range with low polydispersity and negative zeta values (−25 to −46 mV). The partition coefficient of DBC between nanoparticles and water at pH 8.2 was very high (>10^4). EPR (with doxyl-stearate spin labels) data revealed the existence of lamellar arrangements inside the lipid nanoparticles, which was also confirmed by SAXS experiments. Moreover, the addition of DBC increased the molecular packing of both SLN and NLC lipids, indicative of DBC insertion between the lipids, in the milieu assessed by spin labels. Such structural information brings insights into understanding the molecular organization of these versatile drug-delivery systems which have already demonstrated their potential for therapeutic applications in pain control.

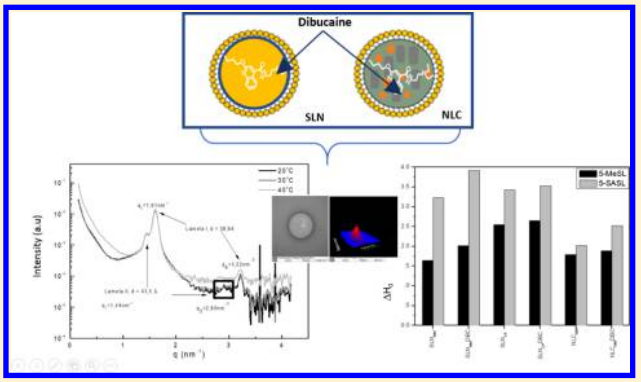

INTRODUCTION

Nanostructured systems have been extensively investigated for anesthetic encapsulation aiming both to increase bioavailability and to decrease local anesthetic toxicity. Solid lipid nanoparticles (SLNs) and nanostructured lipid carriers (NLCs) offer an innovative alternative for the sustained release of local anesthetics.[1−6] The development of these singular nanocarriers, however, demands careful structural characterization to identify the relevant architectural parameters, which could improve the biological response. This understanding is fundamental in building a rationale toward more efficient drug formulations.[7]

SLNs usually have poor drug-loading efficiency, and a drug expulsion is observed during storage. This drawback (drug leakage) is due to the rearrangement of the crystalline lipid core from a high-energy state to a more ordered (β) state on storage.[8] Conversely, NLCs are less-ordered structures with higher drug loading and demonstrate good stability throughout their shelf life. NLCs differ from SLNs, in that a liquid lipid (at ambient temperature) is added to the solid lipid during

Received: July 29, 2018
Revised: October 1, 2018
Published: October 9, 2018

   DOI: 10.1021/acs.langmuir.8b02559
Langmuir 2018, 34, 13296−13304

preparation, favoring the formation of imperfections in the lipid matrix.[9] This increases the intraparticle spaces available to the drug, resulting in greater encapsulation efficiency. It is the amorphous nature of NLCs that can reduce or avoid drug expulsion during storage.[10−12] Recent works demonstrated that SLNs and/or NLCs are suitable nanocarriers for the incorporation of lipophilic drugs such as dibucaine (DBC), benzocaine, lidocaine, tetracaine, etomidate, and prednisolone.[1,2,13,14]

DBC is an amine-amide-type local anesthetic used for pain relief. It is one of the most potent long-lasting local anesthetics, being 15 times more potent than procaine.[15−17] As other anesthetic agents, DBC reversibly blocks nervous transmission when applied to a specific region of the body, but it has limited water solubility—and this property restricts its use by the infiltrative route—and induces systemic toxicity.[15]

The amine group of DBC has a pK_a of 8.3,[18] which enables it to exist in both charged (protonated) and neutral (nonprotonated) forms at pH 7.4. Despite the voluminous isoquinoline ring of DBC, both ionization forms were found to interact with lipid bilayers, increasing the mobility of acyl chains and changing the polar heads of lipids[19] in liposomes.

Other lipid-based nanocarriers are rather complex and understudied. Therefore, developing further knowledge about the soft core of SLNs and NCLs and organization has important implications in drug delivery. Therefore, a detailed characterization of lipid nanocarrier organization should be pursued. Structural insights should bring precious understanding to these versatile systems, which have already demonstrated a great potential for future therapeutic applications in pain control.

EXPERIMENTAL SECTION

Materials. DBC, poloxamer 188 (Pluronic F68), 5-doxyl-stearic acid, and methyl-5-doxyl-stearic acid spin labels (5-SASL and 5-MeSL, respectively) were obtained from Sigma-Aldrich (St. Louis, MO). Myristyl myristate (MM) and cetyl palmitate (CP) were from Dhaymers Fine Chemicals (Brazil) and Croda (Brazil), respectively. Liponate GC (a liquid lipid composed of a mixture of capric and caprylic acids) was supplied by Lipo do Brasil (Brazil). Other reagents used were of high-performance liquid chromatography (HPLC) grade: acetonitrile (J.T. Baker, USA), triethylamine (VETEC, Brazil), and orthophosphoric acid (Ecibra, Brazil). Deionized water (18.2 MΩ cm) was obtained from a Waters ultrapure water system.

Methods. *Preparation of the Lipid Nanoparticles: SLNs and NLCs.* Lipid nanoparticles (SLNs and NLCs) were produced by high pressure and hot homogenization.[14] Both SLNs and NLCs used in this study were prepared using either MM or CP at 2%, w/v. In the case of NLCs, Liponate GC was used, at 0.5 w/w % of the total lipid weight. Briefly, lipids in the absence and presence of DBC (1 mg/mL) were heated to 49 or 64 °C, that is, 10 °C above the melting point of MM (39 °C) and CP (54 °C), respectively. To form a microemulsion, the warmed lipid phase was added to a hot aqueous solution of poloxamer 188 (at 0.5 or 1.5 w/v % for SLNs and NLCs, respectively), under high agitation (10 000 rpm) in an Ultra-turrax T18 (IKA Werke Staufen, Germany) for 3 min. All samples were further homogenized in a Panda 2k (Niro Soavi, Italy) equipment, with three 600 bar cycles, and the formulations were cooled and stored at 4 °C.[20−23]

Determination of Size, Polydispersity, and Zeta Potential. Particle size distribution and visual information of nanoparticles were obtained by nanoparticle tracking analysis, NTA (NanoSight LM20 and NTA 2.0 Analytical Software, NanoSight, Wiltshire, UK). Diluted SLN or NLC samples (0.5 mL; 1:5000 in Milli-Q water v/v) was injected into the chamber with a syringe, and samples were illuminated by a diode laser (635 nm wavelength). The Brownian motion of the individual particles was obtained in real time via a charge-coupled device (CCD) camera and analyzed using NTA 2.0 Analytical Software (NanoSight, UK). Each video clip was captured for 10 s at 25 °C.[24] Measures of the width of the distribution of particle size (span) values were calculated by eq 1

$$\text{Span} = \frac{(D_{0.9} - D_{0.1})}{D_{0.5}} \tag{1}$$

where $D_{0.9}$, $D_{0.5}$, and $D_{0.1}$ are the particle diameters determined, respectively, at the 90th, 50th, and 10th percentile of undersized particles.[25] The zeta potential was measured (at 25 °C) using capillary cells (10 mm with path lengths) in a Malvern Instruments Zetasizer Nano ZS (Worcestershire, UK). All samples were diluted in a solution of 0.1 mmol·L^{-1} sodium chloride before analysis (sample/NaCl water ratio of 1:100, v/v). The number of nanoparticles per mL of colloidal suspension analysis did not change when the samples were prepared with DBC. The results were expressed as the average ± standard deviation of three separate determinations, conducted 1 day after preparation.

Transmission Electron Microscopy. The morphologies of the nanoparticles (SLN_{MM} and SLN_{CP} for SLNs composed of MM and CP, respectively) and NLC_{MM} (NLCs based on MM) with and without DBC were examined using transmission electron microscopy (TEM) (Zeiss LEO-906, 60 kV). Each sample (40 μL) was added to a copper grid with 200 mesh (Electron Microscopy Sciences) and left to rest for about 15 min. One drop of uranile solution (2%, m/m) was then added to improve the contrast of pictures obtained. Any excess of this solution was removed with a filter paper.[26]

Partition Coefficient Determination. The partition coefficient (P) of DBC between nanoparticles and water was determined by phase separation (filtration−centrifugation): 0.3 mL of an SLN or NLC sample diluted in Milli-Q water (2:100 v/v) was transferred to a filtration unit with 10 kDa (Millex Millipore) and centrifuged for 20 min (4100g, in a MC 12 V Sorvall centrifuge). The free DBC in the supernatant was quantified by HPLC, as described in ref 5.

The partition coefficient of DBC, that is, the anesthetic ratio between two immiscible phases [the lipid phase (l) and water phase (w)], was calculated using eq 2

$$P = \frac{n_l/v_l}{n_w/v_w} \tag{2}$$

where n = the number of moles of DBC and v is the volume of phases. The total number of moles of DBC in the sample was obtained from the sum of n_l and n_w. The lipid density was considered to equal 1 g·mL^{-1} to estimate the volume of the lipid phase[16] corresponding to 20 mg·mL^{-1} of MM or CP (total the amount of solid lipid).

Fourier Transform Infrared Spectroscopy. SLNs and NLCs (with and without DBC) were frozen (dry ice/ethanol bath) and lyophilized (Labconco, Freeze Dry System/FreeZone 4.5) over 24 h. A PerkinElmer 100 Fourier transform infrared spectrometer was used; the frequency range was 400−4000 cm^{-1} with 32 scans per sample. The sample (1 mg) was mixed with solid potassium bromide and placed under pressed with a pressure of 10 tons using a hydraulic press to obtain transparent and thin pellets.

Small-Angle X-ray Scattering Measurements. Small-angle X-ray scattering (SAXS) experiments were performed at the National Laboratory of Synchrotron Light (LNLS, Campinas, Brazil) with a radiation wavelength of 1488 Å. The samples were studied using a detector distance of approximately ∼1000 mm. The scattering curves were corrected (background-subtracted). The scattering vector (q) was measured according to eq 3

$$q = \frac{4\pi}{\lambda} \operatorname{sen} \theta \tag{3}$$

where 2θ is the scattering angle and λ is the wavelength of X-rays.

The sample exposure times varied from 2 to 5 min. The SLN_{CP} sample was subjected to a heating process (30, 35, 40, and 45° C), which was performed using a water bath under the thermostatic control. The remaining samples (SLN_{MM}, SLN_{MM}DBC, and

DOI: 10.1021/acs.langmuir.8b02559
Langmuir 2018, 34, 13296−13304

SLN_{CP}DBC) were only run at room temperature. The dimensional information was aimed at the identification of lamellar arrangement, as well as their periodicity (structural organization) and crystalline or amorphous composition.[27,28]

Electron Paramagnetic Resonance Experiments. The lipid milieu of SLNs and NLCs was analyzed from the spectra of two spin probes 5-SASL and 5-MeSL—of slightly different polarities that were incorporated into the nanoparticles (SLN_{MM}, SLN_{CP}, and NLC_{MM}) with and without DBC, up to 1 mol % (relative to total lipid concentration). Each spin label was incubated with the sample for approximately 30 min at 37 °C, and the electron paramagnetic resonance (EPR) spectra were recorded using a Bruker EMX spectrometer (Bruker BioSpin GmbH, Billerica) at 25 °C and also from 5 to 55 °C. The order parameter (S), giving information on the orientation of the lipid core, considering lamellar structures, where the spin-label-long molecular axis is roughly parallel to the normal bilayer, was calculated from the 5-SASL spectra, according to eq 4[29]

$$S = \frac{2A_{//} - 2A_{\perp}}{2[A_{zz} - (A_{xx} + A_{yy})/2]} \quad (4)$$

where $A_{//}$ and $A_{\perp}$, measured directly from the EPR spectrum, are the hyperfine splitting for the spin label's long molecular axis oriented parallel and perpendicular, respectively, to the external magnetic field. A_{zz} (32 Gauss), A_{xx} (6 Gauss), and A_{yy} (6 Gauss) were the principal components of the hyperfine tensor measured in a single crystal.[30] In lipid vesicles (liposomes), S describes the degree of organization in the bilayer, with values from 0 to 1, the unit revealing perfect anisotropy (long molecular axis parallel to the bilayer normal).[31]

The spectra of 5-MeSL were analyzed in terms of an empirical parameter, ΔH_0 (width of the central line).[15] This parameter reports the contribution of both order and mobility in the spectra of spin label inserted into lipid phases. Lower ΔH_0 values correspond to lower order, higher mobility, or both. From here onward, the term organization will be employed to refer to the sum of both contributions.[31,32]

Statistical Analysis. Statistical evaluation of the size distribution used T (Student) test, with a significant level of 5% ($p < 0.05$). The data were analyzed using InStat v.3 (GraphPad Software, Inc., San Diego, CA, USA).

RESULTS AND DISCUSSION

Nanoparticle hydrodynamic diameters (in the absence and presence of DBC) were evaluated by nanoparticle tracking analysis, NTA (Table 1). In this technique, all particles were visualized by video recording (10 s) using a CCD camera. In the video frames, the largest particles are seen as defined bright dots and the smaller particles move more quickly because of the Brownian motion of the particles.[24,33] Different light scattering intensities were observed for each formulation, but the cumulative data in percentile of the particle distribution indicated diameters of homogeneous size, that is, compatible with a single population of particles.

Table 1. Average Sizes (Cumulative Data of the Diameter) of the Lipid Nanoparticles Prepared by High-Pressure Homogenization, as Determined by NTA[a]

	cumulative distribution of diameters (D)				
samples	D_{10} (nm)	D_{50} (nm)	D_{90} (nm)	average diameter (nm)	span
SLN_{MM}	118	178	248	172.00 ± 7.81	0.7
SLN_{MM}DBC	119	174	243	175.67 ± 10.69	0.7
SLN_{CP}	96	181	255	173.33 ± 5.13	0.9
SLN_{CP}DBC	80	148	234	178.00 ± 9.54	1.0
NLC_{MM}	134	178	242	178.67 ± 8.96	0.6
NLC_{MM}DBC	120	168	220	170.67 ± 3.79	0.6

[a] D_{10}, D_{50}, and D_{90} refer to the diameters taken from the 10, 50, and 90% of the cumulative distribution of particles. Statistical analysis: Student T test, $p < 0.05$, $n = 3$.

The polydispersity of nanoparticles measured from the span index (eq 1, where the lower the span the narrower is the particle size distribution[34]) was ≤1, confirming the homogeneity of the system. The size and low polydispersity of the particles measured by NTA are also in accordance with the data obtained by dynamic light scattering.[5] Furthermore, there were no significant differences in particle size upon DBC addition (Table 1). Total concentration of nanoparticles per milliliter laid between 2.46×10^8 and 7.7×10^8 in all formulations.

The steric stabilization provided by the nonionic surfactant Pluronic F68 on the surface of the nanoparticles lead, in the absence of DBC, to zeta potentials in the range of −25 to −46 mV (Table 2). These values were enough to prevent nanoparticle aggregation and to ensure its stability.[23] These results are consistent with those obtained by other research groups,[23,35] which produced SLN with a similar range of negative zeta values, that showed physical stability over 2 years of storage, justified by the addition of suitable steric stabilizers.[36] The results presented in Table 2 also indicate that the surface of the nanoparticles become less negative when DBC is added to both SLNs and NLCs. Because the pK_a of DBC is 8.3;[18] a significant amount of the positively charged anesthetic is present in the formulation (pH = 8.2), and it is reasonable to think that at least a fraction of DBC+ lies in the surface of the nanoparticles,[18] turning the zeta potentials more positive.

Table 2. Zeta Potential of the Nanoparticles (SLNs and NLCs, with and without DBC), Prepared with CP or MM by High-Pressure Homogenization; $n = 3$

sample	zeta potential (mV)
SLN_{MM}	−26.91 ± 7.72
SLN_{MM}DBC	−18.47 ± 2.55
SLN_{CP}	−45.93 ± 4.64
SLN_{CP}DBC	−3.89 ± 0.96
NLC_{MM}	−28.83 ± 4.41
NLC_{MM}DBC	−14.89 ± 2.78

The morphology of SLN_{MM}, SLN_{CP}, and NLC_{MM}, particles was found to be very similar: approximately spherical, with well-delineated contours, and homogeneous size distribution in the range of 200−250 nm (Figure 1). Incorporation of DBC did not affect the morphology or size of the nanoparticles, as exemplified for NLC_{MM} (Figure 1). Moreover, the micrographs also confirmed the results obtained by NTA, regarding the size of the nanoparticles.

It is known that higher the aqueous solubility, the faster the anesthetic distributes and reaches the biological membrane, being more rapidly removed from the site of action, favoring the cessation of the pharmacological effect. On the other hand, the higher the lipid solubility of the anesthetic agent, the greater is its penetration in the nerve membrane, where they concentrate and exert their biological effect.

In that sense, the partition coefficients (P) of DBC between the oily (SLNs or NLCs) and aqueous phases were determined, according to eq 2. The obtained P values were high and statistically different between SLN and NLC

DOI: 10.1021/acs.langmuir.8b02559
Langmuir 2018, 34, 13296−13304

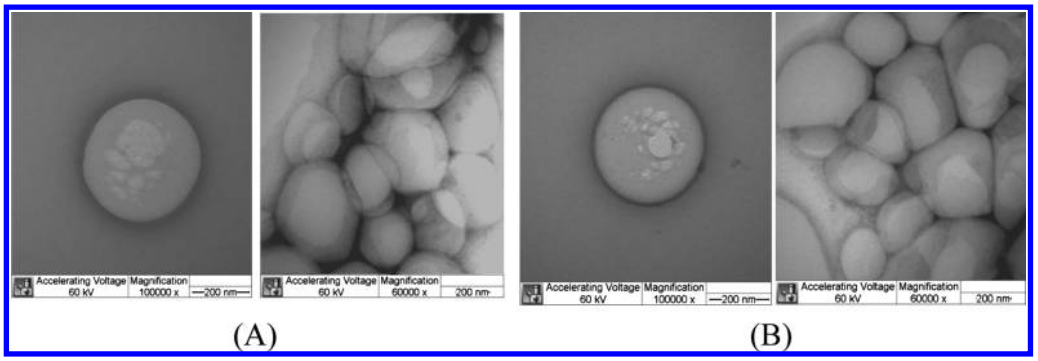

Figure 1. TEM micrographs of the SLNs prepared by high-pressure homogenization: (A) NLC_{MM} and (B) $NLC_{MM}DBC$. Magnification of 100 000× (left) and 60 000× (right).

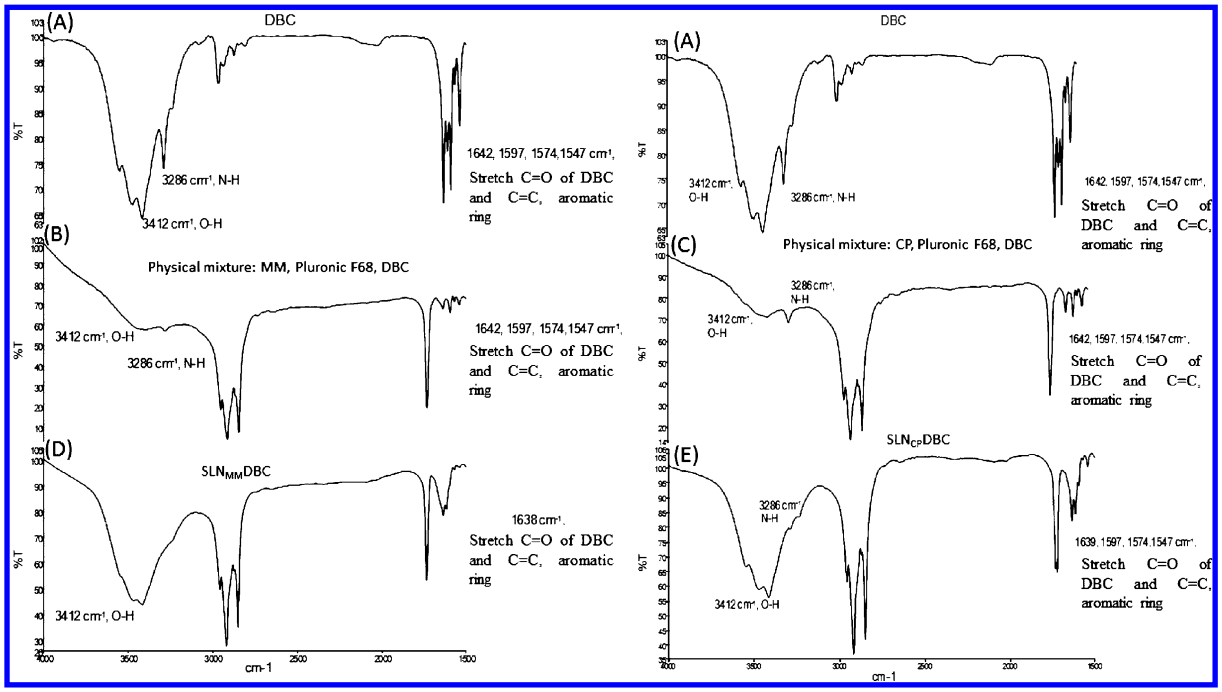

Figure 2. FTIR spectra (in KBr pellets) of DBC (A); its physical mixture with the SLN components: MM (B) or CP (C) plus Pluronic F68 and DBC, $SLN_{MM}DBC$ (D), and $SLN_{CP}DBC$ (E).

nanoparticles (ANOVA, Tukey–Kramer test, $p < 0.05$): 11 510 ± 3949 for $SLN_{MM}DBC$, 13 225 ± 4954 for $SLN_{CP}DBC$, and 31 527 ± 3487 for $NLC_{MM}DBC$.

High *P* values are desirable because they are directly correlated with the anesthetic potency of the formulation.[37,38] Moreover, the *P* values determined here are 1 order of magnitude higher than those reported for other lipid-based drug delivery systems (egg phosphatidylcholine liposomes: 1920 at pH 7.4[19]), attesting the extraordinary loading efficiency of SLNs and NLCs over liposomes. Additionally, NLCs (containing a blend of lipids in their core) produce less crystalline structures than SLNs, being more stable over the time.[9,39] As expected, the partition of DBC between $NLC_{MM}DBC$/water is 2–3 times higher than that between $SLN_{MM}DBC$/water, confirming the high drug loading[40] of the first.

As a first approach to gain an insight into the interaction of DBC with the nanoparticles, Fourier transform infrared (FTIR) spectroscopy was used. The FTIR spectra of free DBC, the physical mixture of the SLN components plus DBC (Figure 2B,C), $SLN_{MM}DBC$ (Figure 2D) and $SLN_{CP}DBC$ (Figure 2E) revealed that the main absorption bands of DBC were observed in all of the samples.

However, comparing the spectra of DBC in the physical mixture and SLN formulations, there were no significant displacements of the main DBC bands (stretching bands: O–H at 3412 cm^{-1}; N–H at 3286 cm^{-1}, C═O at 1642–1574 cm^{-1}, and quinoline ring C═C at 1547 cm^{-1}), suggesting a weak interaction between the drug and the SLNs, probably because DBC was only dissolved in the lipid matrix. Similar observations were reported by Araújo and co-workers[41] for NLCs associated with triamcinolone, suggesting that no chemical interaction took place between the corticosteroid and the lipid matrix, and that triamcinolone was just dissolved in the lipid matrix of the particle.

A multiple-phase system such as SLNs and NLCs, with different densities of electrons and nanometric dimensions, can be dissected by X-ray scattering techniques, which provides important information as to their molecular organization. The peaks observed in SAXS diffractograms are associated with the presence of ordered phases, such as liquid crystals, for example. From the peak position, one can calculate the *repeat* distances

DOI: 10.1021/acs.langmuir.8b02559
Langmuir 2018, 34, 13296–13304

and finally obtain the frame type of the system.[27] Consequently, the use of the SAXS aimed at a better understanding of the structural organization of the lipids that form the core of SLNs and NLCs. Figure 3A shows the

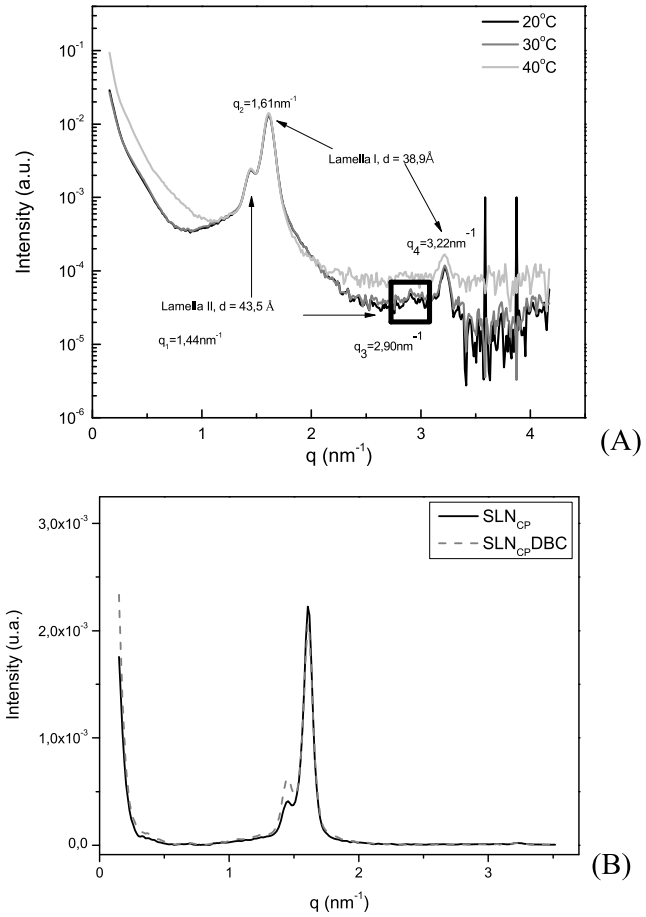

Figure 3. SAXS: scattering intensity vs q vector in: (A) $SLN_{CP}DBC$, measured at increasing (20, 30, and 40 °C) temperatures, and (B) in a SLN_{CP} sample, with and without DBC, measured at 20 °C.

scattering intensity curve, as a function of the scattering q vector, for the $SLN_{CP}DBC$ sample. Two peaks could be observed at 1.61 and 1.44 nm^{-1}, with repeating intervals. These peaks are characteristic of the CP nanoparticles and therefore represent the specific arrangements of the CP lipids within the nanoparticles. The peaks are located at periodic distances, with the same repeat interval, being compatible with the arrangement of a multilamellar lipid structure.[28] Moreover, they have the bilayer core-to-bilayer core distances of 38.9 Å (lamellar phase I) and 43.5 Å (lamellar phase II) (Figure 3A).

The existence of lamellar arrangements inside SLNs/NLCs may sound strange because this requires the presence of water molecules inside the nanoparticle. For example, if we take serum lipoproteins as a model, whose lipid core is formed by triglycerides and cholesterol-esters,[42] these nonpolar molecules form lipid droplets inside the particles. However, that is not the case with SLNs and NLCs. The hydrophilic−lipophilic balance of MM and CP (the major components of the lipid core) is significant, explaining why these lipids would not be comfortable in the absence of water. Despite the crystalline organization of solid lipids inside SLNs described by calorimetric measurements, evidence pertaining to the existence of lamellar lipid phases inside SLNs was also available in the literature.[27,28,43−45] For instance Lukowski and co-workers[27] and de Souza et al.[28] demonstrated by SAXS that CP, as well as stearic acid lipids, are organized in lamellae inside SLNs. These authors also suggested that compounds incorporated into SLNs could be stored between these bilayers. Figure 3A shows that at fixed temperatures, below 30 °C, structural changes were observed. However, above this temperature, just small changes were visualized (e.g., the disappearance of a peak at q_3 = 2.9 observed in curves performed at 30 °C and a reduction in the intensity of formed peaks), but without compromising the internal structure of the particle (Figure 3A). There were no changes in the SAXS diffractograms of SLNs measured in the absence or in the presence of DBC (Figure 3B).

EPR was another spectroscopic technique employed to identify the effect of DBC on the mobility and organization of the lipid core of the nanoparticles. For that purpose, stearic acid-derivatives spin labels (5-SASL and 5-MeSL) were inserted in the lipid milieu of SLNs and NLCs to monitor the molecular arrangements of MM and CP.

Because SAXS results gave indications as to the existence of bilayers inside the nanoparticles, we have applied EPR concepts on the membrane (bilayers) structure to obtain information about DBC effect inside the lipid core of SLNs and NLCs. In membranes at high temperatures, if the degree of order of the bilayer is small, the external extremes in the spectrum are not resolved and the order parameter cannot be directly measured. In this case, one can monitor the width of the central line (ΔH_0), a measure indirectly related to the bilayer fluidity. Therefore, ΔH_0 is a parameter resulting from the orientation and rotational mobility contribution of the spin label inserted into a bilayer.[30]

As for the 5-doxyl stearate spin label (5-SASL), when inserted in bilayers, it monitors regions closer to the polar head group because of the high polarity of the stearic acid.[46] The spectra of 5-SASL in SLN_{MM} and SLN_{CP} are given in Figure 4, whereas Figure 5 depicts the changes in H_0 as a function of temperature.

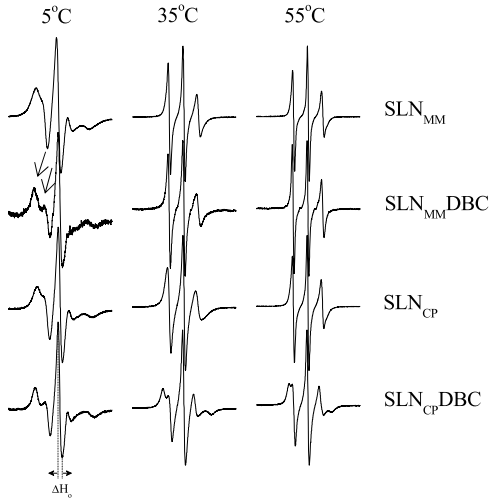

Figure 4. EPR spectra of 5-SASL incorporated in SLN_{MM} and SLN_{CP} in the absence and presence of DBC (molar ratio of 16:1 for MM/DBC and 13:1 for CP/DBC) measured at different temperatures. Total spectra width 100 G. The central field line width, ΔH_0, is indicated.

DOI: 10.1021/acs.langmuir.8b02559
Langmuir 2018, 34, 13296−13304

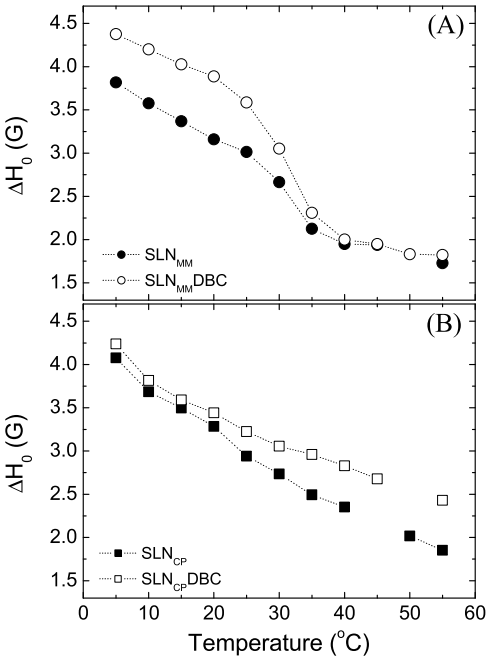

Figure 5. Center field line width, ΔH_0, from EPR spectra of 5-SASL incorporated in: (A) SLN_{MM} and (B) SLN_{CP}, in the absence and presence of DBC (molar ratio of 16:1 for MM/DBC and 13:1 for CP/DBC) at all studied temperatures (from 5 to 55 °C).

The spectra on Figure 4 reveal a high degree of anisotropy below 30 °C and are compatible with the bilayer arrangement,[47] confirming the SAXS data. The second lane of Figure 4 shows that the presence of DBC broadens the SASL signal in SLN_{MM}, increasing ΔH_0 at temperatures below 30 °C (first lane, left spectrum), which indicates a higher degree of anisotropy in the chemical ambience monitored by the spin label. The effect of DBC in the spectrum of 5-SASL is even more evident at lower temperatures (5, 10 °C), where there is a separation in the low-field peak components, as indicated by the arrows over the spectrum. The opposite is seen at temperatures above the melting temperature of MM (39 °C): from 40 to 55 °C, the presence of DBC favors the isotropy of lipids in the region monitored by 5-SASL, leading to minor values of ΔH_0 (Figure 5). Such results reveal a biphasic effect for DBC over SLN_{MM} particles: increasing the lipid milieu order below the melting point of the lipid that forms the SLN core and fluidizing the bilayer arrangement above it.

This effect was confirmed when 5-SASL was incorporated into SLN_{CP}, with and without DBC (Figure 4, third and fourth lanes, and Figure 5).[31] Because the melting point of CP is higher (54 °C) than that of MM,[25,28,48] DBC only induced the widening of the spectra because the measurements were carried out below the melting point of CP.

We have also measured the segmental order parameter (S) in the 5-SASL spectra inserted in SLNs and NLCs. The order parameter of SLN_{CP} at 20 °C (S = 0.62) was greater than that of SLN_{MM} (S = 0.47), indicating higher lipid packing in the nanoparticles composed of CP, as expected because of its longer acyl chain length (regarding MM). As evidenced by the increased ΔH_0 observed below 30 °C (Figure 5), the S values measured at 20 °C in the presence of DBC increased to 0.66 for SLN_{MM}DBC and 0.68 for SLN_{CP}DBC, confirming the higher degree of anisotropy in the chemical ambience monitored by the spin label. Therefore, the presence of DBC determines a rearrangement of the lipids in the SLN core, increasing the molecular orientation of both MM and CP bilayers. These EPR results provided unequivocal evidence of the insertion of DBC into the core region of both MM and CP SLNs, as monitored by the 5-SASL paramagnetic probe.[31]

EPR spectra were also run for NLC samples. As expected, the mix of liquid lipids with MM and CP determined a less organized arrangement in the NLC lipid core, curbing the measure of S values in those nanoparticles. Figure 6 put together the EPR results (ΔH_0 values) measured in the spectra of the spin labels 5-SASL and 5-MeSL incorporated in the different nanoparticles (SLN_{MM}, SLN_{MM}DBC, SLN_{CP}, SLN_{CP}DBC, NLC_{MM}, and NLC_{MM}DBC) at 25 °C. 5-MeSL is the methyl ester of 5-SASL, and in liposomes, it monitors deeper regions of the bilayer.[47] As expected, 5-MeSL (Figure 6, left), being less polar than 5-SASL (Figure 6, right), is inserted deeper into the nanoparticles' bilayers, resulting in more isotropic spectra (narrower and less separated spectral lines) than those of 5-SASL. Both labels detected the partition DBC into SLN and NLC bilayers, increasing the molecular packing at lower temperatures. However, 5-SASL was more sensitive to the effect of DBC than 5-MeSL, indicating that DBC preferentially inserts in the vicinity of the polar head group region of the bilayers.

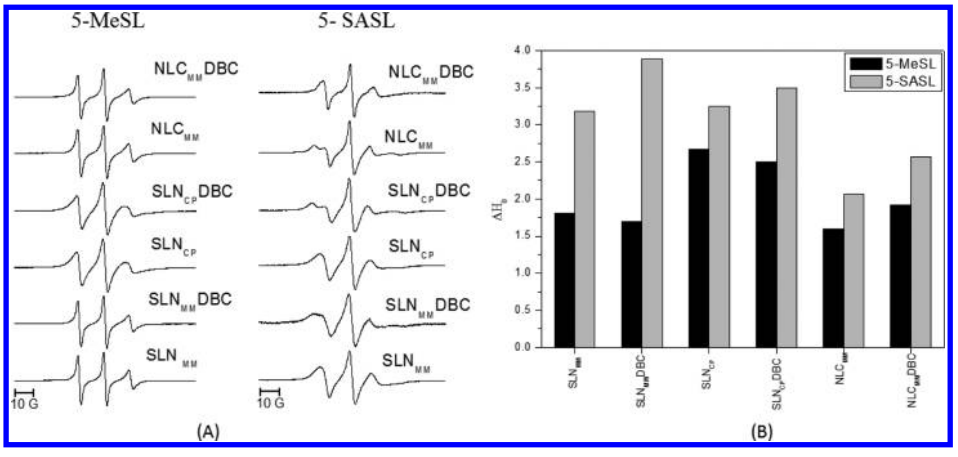

Figure 6. (A) EPR spectra and (B) ΔH_0 values in the spectra of 5-SASL and 5-MeSL inserted into SLN_{MM}, SLN_{MM}DBC, SLN_{CP}, SLN_{CP}DBC, NLC_{MM}, and NLC_{MM}DBC at 25 °C.

DOI: 10.1021/acs.langmuir.8b02559
Langmuir 2018, 34, 13296−13304

In lamellar systems such as liposomes, the spectra of 5-MeSL monitor a less structured region than 5-SASL, which is assigned to its deepest insertion into the bilayer to a less organized region.[15,49] Also in bilayers, a 5-MeSL spin label was used to monitor the effect caused by the partition of the neutral form of different local anesthetics in egg phosphatidylcholine liposomes.[15] All of the nine ester and amino-amide anesthetics, including DBC, caused a decrease in ΔH_0 values when inserted to the same molar ratio (1:3 anesthetic/lipid) in the bilayer. However, only when the membrane was treated with high amounts of the amino-ester type (chlorprocaine, procaine, and tetracaine) anesthetics, the appearance of an additional spectral component was detected, accompanied by a lower anisotropy. This additional spectral component, more immobilized and observed here in the SLN_{MM}DBC sample below 35 °C (Figures 4 and 6), was assigned to the spin label partitioning into a lipid-phase enriched with anesthetics, responsible for the largest local lipid packaging. It is worthwhile noting that the protonated form of DBC has aggregative properties[19] and that atomic force microscopy data evidenced the formation of mixed (bilayer-micelle) structures when DBC was added to planar membranes of dimyristoyl phosphatidylcholine.[18]

Therefore, EPR data revealed that DBC partitions in all formulations studied, caused an increase in the molecular organization of lipids at the inner lipid core of the particles, in the regions monitored by the spin labels (5-SASL and 5-MeSL). Considering that the lipid arrangement within SLN and NLC cores is lamellar (as suggested by SAXS and EPR results), the greatest packaging occurs by DBC insertion between the lipids that comprise the bilayer, within a depth compatible with the position of the labels (that contain a nitroxide radical attached to the fifth carbon of stearic acid or its methyl derivative).

EPR spectra were also used to monitor the stability of the lipid arrangement of SLNs and NLCs upon addition of the anesthetic, following heating and cooling of nanoparticles. The hysteresis of the formulations (SLN_{MM}, SLN_{MM}DBC, SLN_{CP}, and SLN_{CP}DBC) was assessed by evaluating ΔH_0 values of 5-SASL spectra after heating/cooling/reheating cycles. The results showed that in SLN_{MM}, with and without DBC, the chemical environment monitored by the 5-SASL probe is the same, and there is no measurable lipid reorganization (no spectral change) as a function of temperature, but for the transition temperature of the lipid, at ca. 40 °C (data not shown). In SLN_{CP}, a small difference was observed in the measured ΔH_0 after cooling the sample containing DBC, indicating a change in the likely partition of DBC molecules according to the thermal modification of the system. In any case, the change was not significant, such that SLN_{CP} can be considered as a stable formulation in relation to DBC partition.

CONCLUSIONS

In this work, SLNs and NLCs containing DBC were successfully prepared. The lipid nanoparticles were composed of CP or MM as the solid lipid matrices, Pluronic F68 as the steric stabilizer, and contained (NLCs) or not (SLNs) a small proportion of liquid lipid (a triglyceride of capric and caprylic acids). DBC effect on the structural organization of the nanoparticles was also evaluated. Using a high-pressure homogenization method, particles with ca. 200 nm and high drug loading were obtained. DBC partition into SLNs (SLN_{MM}DBC and SLN_{CP}DBC) and NLC_{MM} was very high ($>10^4$), in accordance with the lipophilicity of the anesthetic. SAXS results indicated the existence of lamellar lipid arrangements inside both SLNs and NLCs. FTIR spectra did not provide any evidence of the interaction between DBC and the lipids, but EPR measurements confirmed the lamellar lipid organization of both SLNs and NLCs. It also revealed that DBC partitions into the lipid core of the nanoparticles, promoting greater molecular organization of the lipids, in the moiety monitored by the spin labels (5-SASL and 5-MeSL), at temperatures below the melting point of the solid lipid. The results show the complementation of biophysical and pharmaceutical approaches in the characterization of a potential innovative formulation for the treatment of pain.

AUTHOR INFORMATION

Corresponding Author

*E-mail: m.g.barbosafernandes@gmail.com. Phone: 55 84 996124869.

ORCID

Raquel M. Barbosa: 0000-0003-3798-5512

Notes

The authors declare no competing financial interest.

ACKNOWLEDGMENTS

Financial support for this research was provided by the Fundação de Amparo à Pesquisa do Estado de São Paulo (FAPESP, # 05/00121-9, and 14/14457-5). Raquel M. Barbosa and Eneida de Paula acknowledge fellowships from CAPES and CNPq (Brazil), respectively.

ABBREVIATIONS

5-SASL, 5-doxyl-stearic acid; CP, cetyl palmitate; DBC, dibucaine; EPR, electron paramagnetic resonance; FTIR, Fourier transform infrared spectroscopy; 5-MeSL, methyl-5-doxyl-stearic acid; MM, myristyl myristate; NLCs, nanostructured lipid carriers; *P*, partition coefficient; SAXS, small-angle X-ray scattering; SLNs, solid lipid nanoparticles; TEM, transmission electron microscopy

REFERENCES

(1) zur Mühlen, A.; Schwarz, C.; Mehnert, W. Solid lipid nanoparticles (SLN) for controlled drug delivery - Drug release and release mechanism. *Eur. J. Pharm. Biopharm.* **1998**, *45*, 149−155.

(2) Schwarz, C.; Mehnert, W. Solid lipid nanoparticles (SLN) for controlled drug delivery II. drug incorporation and physicochemical characterization. *J. Microencapsulation* **1999**, *16*, 205−213.

(3) Pathak, P.; Nagarsenker, M. Formulation and evaluation of lidocaine lipid nanosystems for dermal delivery. *AAPS PharmSciTech* **2009**, *10*, 985−992.

(4) Leng, F.; Wan, J.; Liu, W.; Tao, B.; Chen, X. Prolongation of epidural analgesia using solid lipid nanoparticles as drug carrier for lidocaine. *Reg. Anesth. Pain Med.* **2012**, *37*, 159−165.

(5) Barbosa, R. M.; Klassen, A.; Marcato, P. D.; Franz-Montan, M.; Grillo, R.; Fraceto, L. F.; Paula, E. Validation of an HPLC method for the determination of Dibucaine encapsulated in Solid Lipid Nanoparticles and Nanostructured Lipid Carriers. *Lat. Am. J. Pharm.* **2013**, *32*, 1362−1369.

(6) Basha, M.; Abd El-Alim, S.; Kassem, A.; El Awdan, S.; Awad, G. Benzocaine loaded solid lipid nanoparticles: Formulation design, *in vitro* and *in vivo* evaluation of local anesthetic effect. *Curr. Drug Deliv.* **2015**, *12*, 680−692.

(7) Radaic, A.; Barbosa, L. R. S.; Jaime, C.; Kapila, Y. L.; Pessine, F. B. T.; de Jesus, M. B. How Lipid Cores Affect Lipid Nanoparticles as

DOI: 10.1021/acs.langmuir.8b02559
Langmuir 2018, 34, 13296−13304

Drug and Gene Delivery Systems. *Advances in Biomembranes and Lipid Self-Assembly*, 24th ed.; Elsevier, 2016; pp 1−42.
(8) Souto, E. B.; Doktorovová, S. Solid Lipid Nanoparticle Formulations: Pharmacokinetic and Biopharmaceutical Aspects in Drug Delivery. *Methods Enzymol.* **2009**, *464*, 105−129.
(9) Pardeike, J.; Hommoss, A.; Müller, R. H. Lipid nanoparticles (SLN, NLC) in cosmetic and pharmaceutical dermal products. *Int. J. Pharm.* **2009**, *366*, 170−184.
(10) Saupe, A.; Wissing, S. A.; Lenk, A.; Schmidt, C.; Müller, R. H. Solid lipid nanoparticles (SLN) and nanostructured lipid carriers (NLC) – structural investigations on two different carrier systems. *Bio-Med. Mater. Eng.* **2005**, *15*, 393−402.
(11) de Araújo, D. R.; da Silva, D. C.; Barbosa, R. M.; Franz-Montan, M.; Cereda, C. M. S.; Padula, C.; Santi, P.; de Paula, E. Strategies for delivering local anesthetics to the skin: focus on liposomes, solid lipid nanoparticles, hydrogels and patches. *Expet Opin. Drug Deliv.* **2013**, *10*, 1551−1563.
(12) Müller, R. H.; Mader, K.; Gohla, S. Solid lipid nanoparticles (SLN) for controlled drug delivery - a review of the state of the art. *Eur. J. Pharm. Biopharm.* **2000**, *50*, 161−177.
(13) Puglia, C.; Sarpietro, M. G.; Bonina, F.; Castelli, F.; Zammataro, M.; Chiechio, S. Development, characterization, and in vitro and in vivo evaluation of benzocaine- and lidocaine-loaded nanostructrured lipid carriers. *J. Pharm. Sci.* **2011**, *100*, 1892−1899.
(14) Barbosa, R. M.; da Silva, C. M. G.; Bella, T. S.; de Araújo, D. R.; Marcato, P. D.; Durán, N.; de Paula, E. Cytotoxicity of solid lipid nanoparticles and nanostructured lipid carriers containing the local anesthetic dibucaine designed for topical application. *J. Phys.: Conf. Ser.* **2013**, *429*, 012035.
(15) de Paula, E.; Schreier, S. Use of a novel method for determination of partition coefficients to compare the effect of local anesthetics on membrane structure. *Biochim. Biophys. Acta, Biomembr.* **1995**, *1240*, 25−33.
(16) de-Paula, E.; Schreier, S. Molecular and physicochemical aspects of local anesthetic-membrane interaction. *Braz. J. Med. Biol. Res.* **1996**, *29*, 877−894.
(17) Crystal, C. S.; McArthur, T. J.; Harrison, B. Anesthetic and procedural sedation techniques for wound management. *Emerg. Med. Clin.* **2007**, *25*, 41−71.
(18) Malheiros, S. V. P.; Pinto, L. M. A.; Gottardo, L.; Yokaichiya, D. K.; Fraceto, L. F.; Meirelles, N. C.; de Paula, E. A new look at the hemolytic effect of local anesthetics, considering their real membrane/water partitioning at pH 7.4. *Biophys. Chem.* **2004**, *110*, 213−221.
(19) Lorite, G. S.; Nobre, T. M.; Zaniquelli, M. E. D.; de Paula, E.; Cotta, M. A. Dibucaine effects on structural and elastic properties of lipid bilayers. *Biophys. Chem.* **2009**, *139*, 75−83.
(20) Schwarz, C.; Mehnert, W.; Lucks, J. S.; Müller, R. H. Solid lipid nanoparticles (SLN) for controlled drug delivery. I. Production, characterization and sterilization. *J. Controlled Release* **1994**, *30*, 83−96.
(21) Liedtke, S.; Wissing, S.; Müller, R. H.; Mäder, K. Influence of high pressure homogenisation equipment on nanodispersions characteristics. *Int. J. Pharm.* **2000**, *196*, 183−185.
(22) Uner, M. Preparation, characterization and physico-chemical properties of solid lipid nanoparticles (SLN) and nanostructured lipid carriers (NLC): their benefits as colloidal drug carrier systems. *Pharmazie* **2006**, *61*, 375−386.
(23) Mitri, K.; Shegokar, R.; Gohla, S.; Anselmi, C.; Müller, R. H. Lipid nanocarriers for dermal delivery of lutein: preparation, characterization, stability and performance. *Int. J. Pharm.* **2011**, *414*, 267−275.
(24) Filipe, V.; Hawe, A.; Jiskoot, W. Critical evaluation of Nanoparticle Tracking Analysis (NTA) by NanoSight for the measurement of nanoparticles and protein aggregates. *Pharm. Res.* **2010**, *27*, 796−810.
(25) Teeranachaideekul, V.; Souto, E. B.; Junyaprasert, V. B.; Müller, R. H. Cetyl palmitate-based NLC for topical delivery of Coenzyme Q10 - Development, physicochemical characterization and in vitro release studies. *Eur. J. Pharm. Biopharm.* **2007**, *67*, 141−148.
(26) Bozzola, J. J.; Russell, L. D. *Electron microscopy*; Jones and Bartlett Publishers: London, 1999; p 670.
(27) Lukowski, G.; Kasbohm, J.; Pflegel, P.; Illing, A.; Wulff, H. Crystallographic investigation of cetylpalmitate solid lipid nanoparticles. *Int. J. Pharm.* **2000**, *196*, 201−205.
(28) de Souza, A. L. R.; Andreani, T.; Nunes, F. M.; Cassimiro, D. L.; de Almeida, A. E.; Ribeiro, C. A.; Sarmento, V. H. V.; Gremião, M. P. D.; Silva, A. M.; Souto, E. B. Loading of praziquantel in the crystal lattice of solid lipid nanoparticles. *J. Therm. Anal. Calorim.* **2012**, *108*, 353−360.
(29) Jost, P.; Libertini, L. J.; Hebert, V. C.; Griffith, O. H. Lipid spin labels in lecithin multilayers. A study of motion along fatty acid chains. *J. Mol. Biol.* **1971**, *59*, 77−98.
(30) Schreier, S.; Polnaszek, C. F.; Smith, I. C. P. Spin label in membranes. *Biochim. Biophys. Acta, Rev. Biomembr.* **1978**, *155*, 395−436.
(31) Kontogiannopoulos, K. N.; Dasargyri, A.; Ottaviani, M. F.; Cangiotti, M.; Fessas, D.; Papageorgiou, V. P.; Assimopoulou, A. N. Advanced Drug Delivery Nanosystems for Shikonin: A Calorimetric and Electron Paramagnetic Resonance Study. *Langmuir* **2018**, *34*, 9424−9434.
(32) Marsh, D. In *Membrane Spectroscopy*; Grell, E., Ed.; Springer Berlin Heidelberg: New York, 1981; Vol. *31*, pp 51−142.
(33) Hoffmeister, C. R. D.; Durli, T. L.; Schaffazick, S. R.; Raffin, R. P.; Bender, E. A.; Beck, R. C. R.; Pohlmann, A. R.; Guterres, S. S. Hydrogels containing redispersible spray-dried melatonin-loaded nanocapsules: a formulation for transdermal-controlled delivery. *Nanoscale Res. Lett.* **2012**, *7*, 251.
(34) Teeranachaideekul, V.; Souto, E. B.; Junyaprasert, V. B.; Müller, R. H. Cetyl palmitate-based NLC for topical delivery of Coenzyme Q10 - Development, physicochemical characterization and in vitro release studies. *Eur. J. Pharm. Biopharm.* **2007**, *67*, 141−148.
(35) Lai, F.; Sinico, C.; De Logu, A.; Zaru, M.; Müller, R. H.; Fadda, A. M. SLN as a topical delivery system for Artemisia arborescens essential oil: in vitro antiviral activity and skin permeation study. *Int. J. Nanomed.* **2007**, *2*, 419−425.
(36) Mishra, P. R.; Shaal, L. A.; Müller, R. H.; Keck, C. M. Production and characterization of Hesperetin nanosuspensions for dermal delivery. *Int. J. Pharm.* **2009**, *371*, 182−189.
(37) Strichartz, G. R. Local Anesthetics. *Handbook of Experimental Pharmacology*; Springer, 1987; Vol. *81*.
(38) Mclure, H. A.; Rubin, A. P. Review of local anaesthetic agents. *Minerva Anestesiol.* **2005**, *71*, 59−74.
(39) Ruktanonchai, U.; Limpakdee, S.; Meejoo, S.; Sakulkhu, U.; Bunyapraphatsara, N.; Junyaprasert, V.; Puttipipatkhachorn, S. The effect of cetyl palmitate crystallinity on physical properties of gamma-oryzanol encapsulated in solid lipid nanoparticles. *Nanotechnology* **2008**, *19*, 095701.
(40) Rosenblatt, K. M.; Bunjes, H. Evaluation of the drug loading capacity of different lipid nanoparticle dispersions by passive drug loading. *Eur. J. Pharm. Biopharm.* **2017**, *117*, 49−59.
(41) Araújo, J.; Gonzalez-Mira, E.; Egea, M. A.; Garcia, M. L.; Souto, E. B. Optimization and physicochemical characterization of a triamcinolone acetonide-loaded NLC for ocular antiangiogenic applications. *Int. J. Pharm.* **2010**, *393*, 168−176.
(42) Berg, J. M.; Tymoczko, J. L.; Gatto, G. J., Jr.; Stryer, L. *Biochemistry*, 8th ed.; W.H. Freeman: New York, 2015.
(43) Rosenblatt, K. M.; Bunjes, H. Poly(vinyl alcohol) as Emulsifier Stabilizes Solid Triglyceride Drug Carrier Nanoparticles in the α-Modification. *Mol. Pharm.* **2009**, *6*, 105−120.
(44) Radler, J. O.; Koltover, I.; Salditt, T.; Safinya, C. R. Structure of DNA-cationic liposome complexes: DNA intercalation in multilamellar membranes in distinct interhelical packing regimes. *Science* **1997**, *275*, 810−814.
(45) de Jesus, M. B.; Radaic, A.; Hinrichs, W. L. J.; Ferreira, C. V.; De Paula, E.; Hoekstra, D.; Zuhorn, I. S. Inclusion of the helper lipid dioleoyl-phosphatidylethanolamine in solid lipid nanoparticles inhibits their transfection efficiency. *J. Biomed. Nanotechnol.* **2014**, *10*, 355−365.

DOI: 10.1021/acs.langmuir.8b02559
Langmuir 2018, 34, 13296−13304

(46) Marsh, D. Polarity and permeation profiles in lipid membranes. *Proc. Natl. Acad. Sci. U.S.A.* **2001**, *98*, 7777−7782.
(47) Bianconi, M. L.; do Amaral, A. T.; Schreier, S. Use of membrane spin label spectra to monitor rates of reaction of partitioning compounds: hydrolysis of a local anesthetic analog. *Biochem. Biophys. Res. Commun.* **1988**, *152*, 344−350.
(48) Aydın, A. A.; Okutan, H. High-chain fatty acid esters of myristyl alcohol with even carbon number: Novel organic phase change materials for thermal energy storage—1. *Sol. Energy Mater. Sol. Cells* **2011**, *95*, 2752−2762.
(49) Fraceto, L. F.; Pinto, L. d. M. A.; Franzoni, L.; Braga, A. A. C.; Spisni, A.; Schreier, S.; de Paula, E. Spectroscopic evidence for a preferential location of lidocaine inside phospholipid bilayers. *Biophys. Chem.* **2002**, *99*, 229−243.

DOI: 10.1021/acs.langmuir.8b02559
Langmuir 2018, 34, 13296−13304